ACS NANO

www.acsnano.org

Wearable Sweat Biosystem with Dual Diffusion-Limiting Interface for Dynamic Hyperlactatemia Management in Critical Care

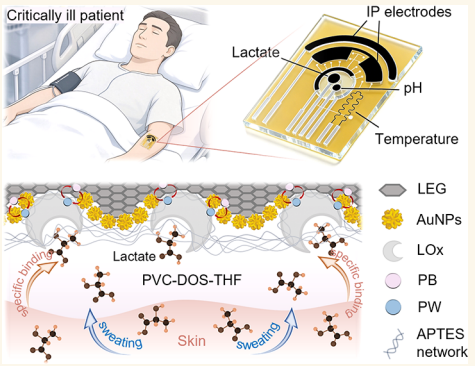
Yunxiang Long,◆ Xiaosen Pan,◆ Yao Chen, Nanpei Li, Wentong Wang, Yuqi Wang, Wanyu Zhang, Taozhe Liu, Qiuting Peng, Kun Yang, Guorui Jin, Chang Liu, Jian Lv, Feng Xu, Kai Qu,* Yunsheng Fang,* Yu Song,* and Ting Lin*

Cite This: *ACS Nano* 2026, 20, 28602−28616

Read Online

ACCESS | Metrics & More | Article Recommendations | Supporting Information

ABSTRACT: **Hyperlactatemia is a critical indicator of tissue hypoperfusion, metabolic dysfunction, and an adverse prognosis in critically ill patients. Yet conventional monitoring depends entirely on intermittent, invasive blood sampling, which cannot capture the dynamic metabolic fluctuations required to guide timely clinical interventions. Herein, we report a wearable sweat-sensing device built on a dual-diffusion-limiting architecture for the continuous and accurate assessment of clinical hyperlactatemia. This system synergistically modulates lactate diffusion in sweat through a silane-network-encapsulated lactate oxidase layer coupled to a polyvinyl chloride layer. This design effectively delays enzyme saturation, extending the linear detection range for sweat lactate to 0−60 mM and thereby fulfilling the stringent requirements of critical care monitoring. The device also integrates real-time pH and temperature calibration to safeguard measurement accuracy in complex physiological environments. Moreover, linear mixed-effects analysis of 82 paired samples from 33 critically ill patients demonstrated a strong association between sweat and blood lactate levels, with a marginal R^2 of 0.840. Sweat lactate effectively identified hyperlactatemia and predicted in-hospital mortality, yielding areas under the receiver operating characteristic curve values of 0.943 and 0.785, respectively. The integrated iontophoresis-microfluidics module further ensures high consistency with bedside arterial blood gas analysis, as validated by a marginal R^2 of 0.811. Together, these results establish sweat biosensors as a promising platform for continuous metabolic monitoring, resuscitation assessment, and objective prognostic stratification in critical care settings.**

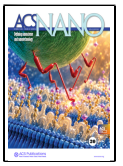


KEYWORDS: *wearable sweat biosystem, electrochemical sensing, dual diffusion-limiting interface, critical care management, hyperlactatemia*

INTRODUCTION

Clinical insults, including malignancy, sepsis, and surgical trauma, frequently trigger immune dysregulation and systemic hypoxia, driving a profound metabolic crisis in an intensive care unit (ICU). This pathological milieu accelerates glycolytic lactate production while impairing hepatic and renal clearance, ultimately leading to hyperlactatemia.[1−4] Beyond serving as a marker of tissue anaerobiosis, hyperlactatemia acts as a powerful, independent predictor of multiple organ dysfunction, prolonged hospitalization, and elevated short-term mortality risk.[5] Importantly, whereas cross-sectional lactate measurements provide only a diagnostic snapshot, the dynamic evolution of lactate clearance offers critical, actionable, real-time insight into resuscitation efficacy.[6] Lactate clearance represents a cornerstone of early goal-directed therapy (EGDT), guiding the precise titration of fluid resuscitation, the fine-tuning of vasopressor support, and the strategic optimization of organ protection.[7−10] However, current clinical lactate monitoring remains limited to invasive, intermittent sampling via arterial blood gas (ABG) analysis. This approach lacks the temporal resolution to capture volatile metabolic shifts during the golden hour of critical care, and inherent procedural risks preclude the continuous, prolonged monitoring indispensable for the rapidly evolving pathophysiology of critically ill patients.[11] Thus, there remains an unmet clinical

Received: July 6, 2026
Revised: September 29, 2026
Accepted: September 30, 2026
Published: October 12, 2026



ACS Publications © 2026 American Chemical Society

https://doi.org/10.1021/acsnano.6c12805
ACS Nano 2026, 20, 28602−28616

Downloaded from pubs.acs.org/ancac3/article-pdf/20/42/28602/6882571 2/acsnano.6c12805.pdf by CITY UNIV OF HONG KONG user on 11 November 2026

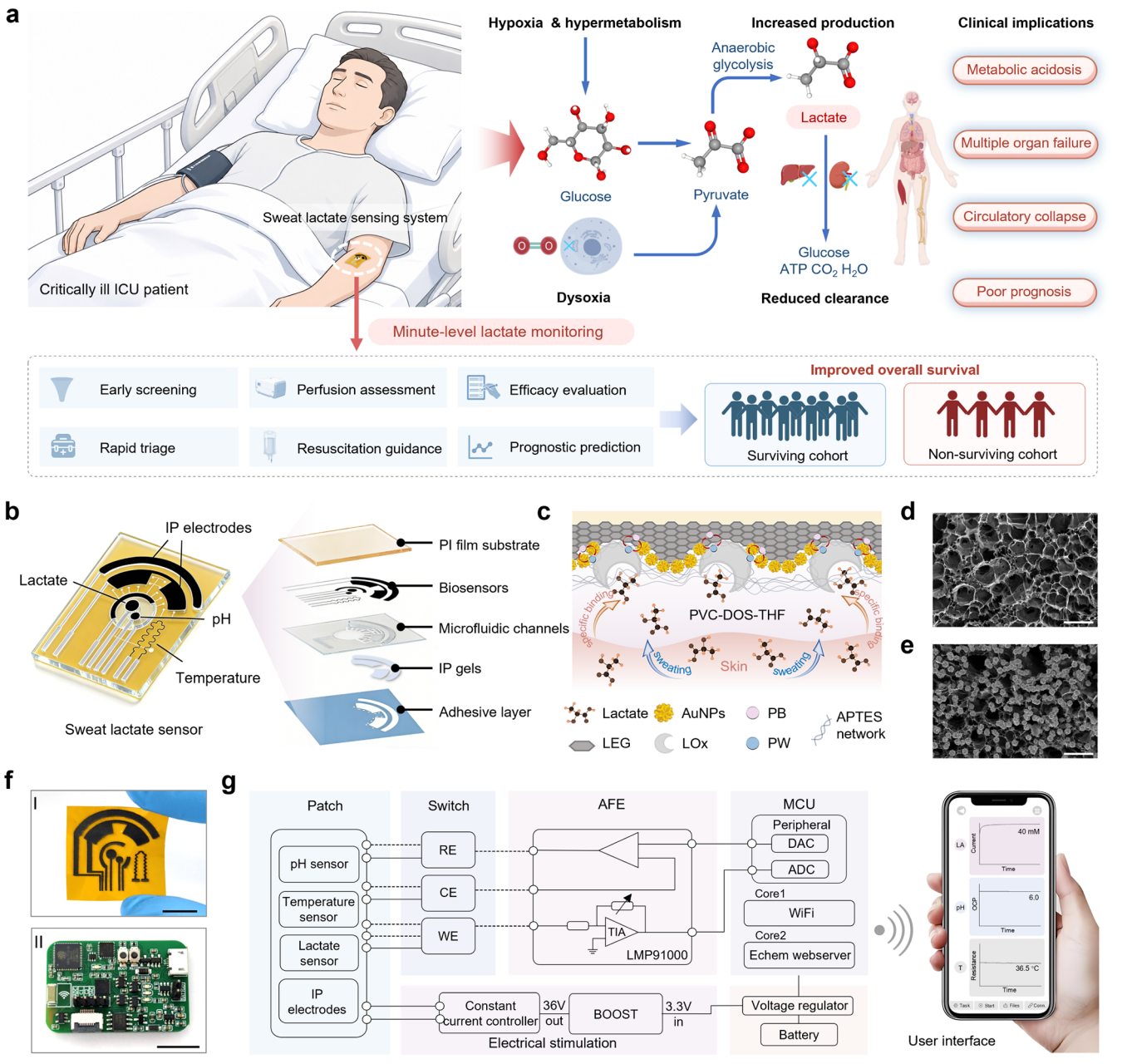


Figure 1. Sweat-sensing platform for noninvasive hyperlactatemia monitoring in intensive care. (a) Pathogenesis of hyperlactatemia in critically ill patients and the clinical utility of minute-level lactate dynamics. (b) Schematic illustration and exploded view of the wearable sweat lactate sensor. IP, iontophoresis. (c) Working mechanism of the lactate biosensor. PB, Prussian blue; PW, Prussian white; PVC-DOS-THF, poly(vinyl chloride)-bis(2-ethylhexyl) sebacate-tetrahydrofuran. (d and e) SEM images of the bare LEG electrode (d) and the AuNP-modified electrode interface (e). Scale bar, 5 μm. (f) Photographs of the sensor array (I) and PCB (II). Scale bar, 1 cm. (g) Block diagram of the integrated electronic system. WE, working electrode; CE, counter electrode; RE, reference electrode; AFE, analog front-end; TIA, transimpedance amplifier; ADC, analog-to-digital converter; DAC, digital-to-analog converter.

imperative to develop continuous, noninvasive lactate monitoring platforms that complement the intermittent, discrete readouts provided by conventional blood-gas assays. By bridging multihour monitoring gaps inherent to periodic blood sampling, such wearable systems enable real-time detection of hyperlactatemia and support timely, targeted therapeutic interventions to optimize critical patient outcomes.[12]

Wearable bioelectronics, characterized by their miniaturization, flexibility, and low power consumption, have emerged as a promising alternative for real-time biomarker diagnostics.[13−15] Specifically, wearable sweat-sensing platforms represent pivotal enabling tools for noninvasive, real-time biochemical profiling.[16] However, translating state-of-the-art laboratory prototypes into clinically deployable devices remains a formidable challenge in critical care. First, the sweat-blood lactate correlation under pathophysiological conditions remains poorly defined, leaving it unclear whether sweat lactate can serve as a high-fidelity blood surrogate for the accurate diagnosis of clinical hyperlactatemia.[17] Additionally, while current lactate sensors exhibit exceptional performance in daily and sports wellness monitoring,[18−21] such performance

https://doi.org/10.1021/acsnano.6c12805
ACS Nano 2026, 20, 28602−28616

Downloaded from pubs.acs.org/ancac3/article-pdf/20/42/28602/6882571 2/acsnano.6c12805.pdf by CITY UNIV OF HONG KONG user on 11 November 2026

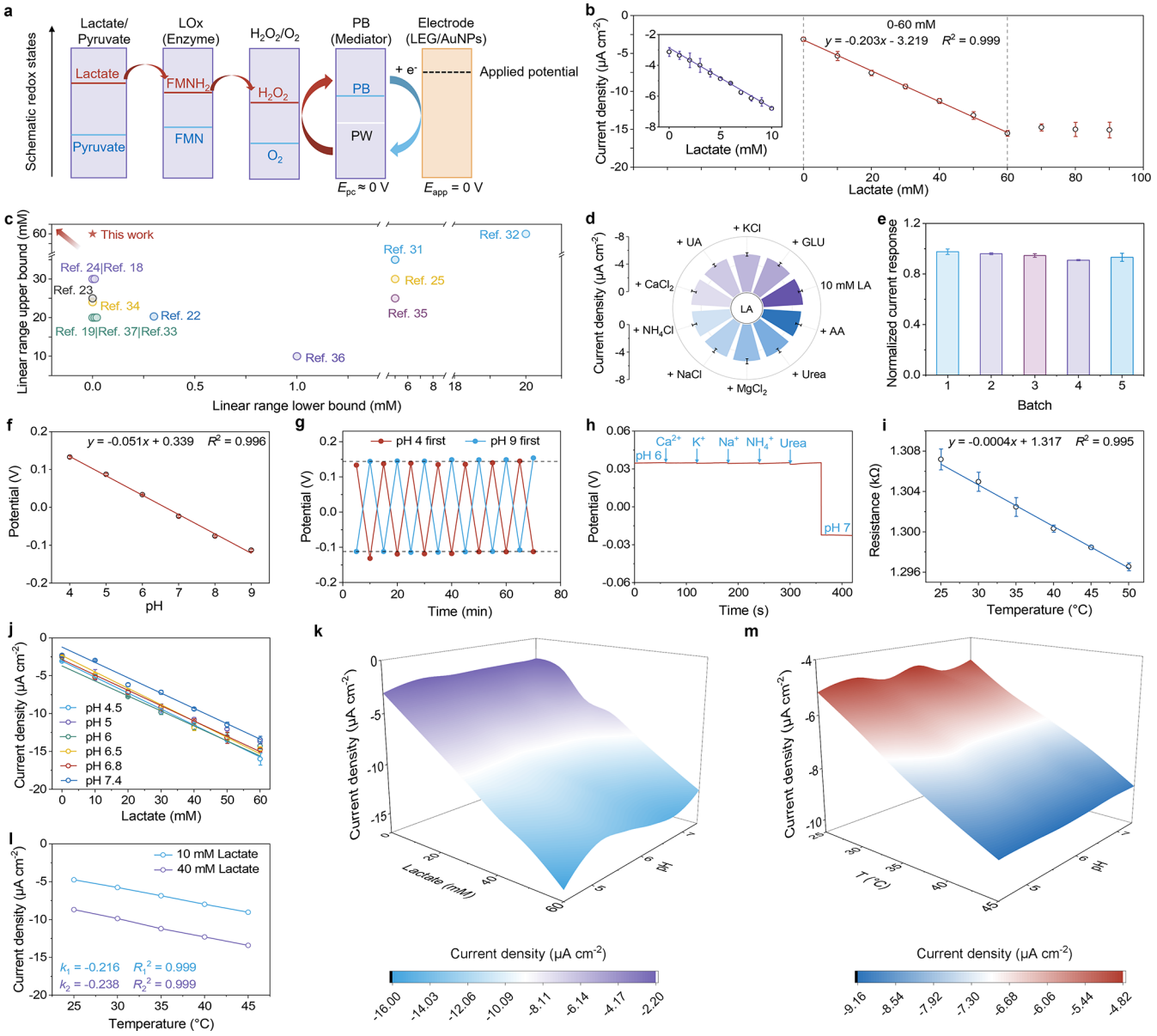


Figure 2. Electrochemical characterization and calibration of sweat lactate sensors. (a) Energy level alignment and electron transfer pathway for lactate sensing. All potentials are reported versus the integrated Ag/AgCl reference electrode. E_{pc}, cathodic peak potential; E_{app}, applied potential. (b) Linear calibration curves for lactate. The linear range is 0−60 mM, with measurements at 60−100 mM illustrating the onset of saturation beyond this range. (c) Comparison of linear range against previously reported wearable lactate biosensors. (d) Selectivity profile against potential interfering species. (e) Reproducibility of the lactate sensor. Normalized current response to 10 mM lactate across five independent fabrication batches. (f) Linear calibration of the pH sensor across varied pH levels. (g) Continuous pH monitoring between pH 4.0 and 9.0 over 70 min. (h) pH selectivity against common interfering ions and metabolites. (i) Linear calibration of the temperature sensor. (j) Lactate sensor calibration plots under varied pH conditions. (k) 3D surface plot illustrating the influence of pH on lactate sensing response. (l) Temperature dependence of the lactate sensor response from 25 to 45 °C. (m) 3D surface plot showing the combined effect of pH and temperature on the response to 10 mM lactate. Error bars represent mean ± SD, n = 3.

does not directly translate to critical care settings, as healthy exercise models fail to recapitulate the complex sudomotor physiology observed in critically ill patients. In the ICU, sweat secretion is profoundly confounded by hemodynamic instability, acid−base disturbances, and polypharmacy, which can severely degrade the reliability of the noninvasive lactate assessment. At the sensor level, strategies such as electrode area enlargement, mediator optimization, enzyme immobilization, and engineered sweat handling have improved lactate sensor performance. However, they generally do not independently control substrate transport at both the enzyme microenvironment and the outer sweat sensor interface. Most reported lactate sensors saturate at concentrations below 35 mM, precluding quantitative linear monitoring of the marked lactate elevations in critically ill patients.[22−25] Meanwhile, intrinsic fluctuations in the sweat matrix, notably sweat secretion rate, pH, and temperature, further destabilize enzymatic lactate sensor performance by inhibiting lactate oxidase activity and interfering with interfacial electron-transfer kinetics.[26,27] Consequently, developing a robust sensing paradigm that integrates an extended linear detection range and multimodal calibration is critical to achieving clinical-grade

https://doi.org/10.1021/acsnano.6c12805
ACS Nano 2026, 20, 28602−28616

Downloaded from pubs.acs.org/ancac3/article-pdf/20/42/28602/6882571 2/acsnano.6c12805.pdf by CITY UNIV OF HONG KONG user on 11 November 2026

precision for noninvasive hyperlactatemia monitoring in critically ill populations.

In this context, we developed a self-calibrating wearable sweat sensor for noninvasive, dynamic hyperlactatemia monitoring, achieving a wide linear detection range of 0−60 mM through a nanostructured electrochemical electrode and a dual-diffusion-limiting interface. The electrodes, fabricated by immobilizing gold nanoparticles (AuNPs) onto laser-engraved graphene (LEG), maximize the electrochemically active surface area to ensure high sensitivity across the broad lactate sensing range. Building upon this design, the sensing interface combines an in situ polymerized (3-aminopropyl)-triethoxysilane-lactate oxidase (APTES-LOx) buffering network with an outer polyvinyl chloride (PVC) layer to mitigate enzyme saturation. The device integrates microfluidic sweat transport with real-time temperature and pH sensors for calibration and stable long-term lactate monitoring. Additionally, a pilot ICU study utilizing mixed-effects modeling shows a strong association between blood and sweat lactate (R^2_m = 0.840), serving as a reliable noninvasive surrogate for identifying hyperlactatemia and predicting in-hospital mortality. Furthermore, the device enables continuous bedside validation in the ICU, maintaining high temporal synchrony with ABG analysis (R^2_m = 0.811). This work presents a robust clinical translation paradigm for the precise monitoring of hyperlactatemia with direct implications for guiding EGDT and optimizing personalized interventions in critical care medicine.

RESULTS AND DISCUSSION

Wearable Sweat Lactate Sensing toward Real-Time Hyperlactatemia Monitoring

As illustrated in Figure 1a, hyperlactatemia is a prevalent metabolic hallmark in critically ill patients, driven by hypoxia, hypermetabolism, and impaired oxygen utilization. These disturbances promote excess lactate production and reduce organ clearance, triggering metabolic acidosis, organ failure, circulatory collapse, and immunosuppression. Minute-level lactate monitoring is critical for enabling comprehensive peri-resuscitation assessment spanning early diagnosis, intervention guidance, and outcome prediction in ICU cohorts, ultimately improving their overall survival (Notes S1, S2 and Figure S1). However, existing monitoring modalities, encompassing conventional discrete blood sampling and invasive bioelectronic alternatives, remain inherently constrained by temporal tracking blind spots, biofouling-induced signal drift, and contraindications specific to critical care settings[28,29] (Note S3). To meet the clinical need for monitoring markedly elevated and fluctuating lactate levels in critical illness, we developed a sweat lactate sensor with a rationally engineered functional interface to enable broad-range linear detection (Figure 1b). The core of our sensing strategy relies on a hierarchical electrode-bioactive layer architecture to mitigate enzyme saturation (Figure 1c and Note S4). Initially, the electrical conductivity of porous LEG electrodes is improved through in situ electrodeposited AuNPs,[27] ensuring robust signal transduction over a wide concentration range (Figures 1d,e and S2 to S4). Next, a Prussian blue-nickel hexacyanoferrate (PB-NiHCF) redox mediator acts as a stable electron-transfer mediator,[30] with a low redox potential near 0 V (Figure S5). Within the bioactive layer, a dual-interface regulation system is constructed by integrating an internal APTES/LOx matrix with an external PVC membrane. The APTES-derived 3D polysiloxane network ensures enzyme stability while introducing steric hindrances that modulate lactate access to active sites. The dense PVC membrane tunes the sensing kinetics by shifting the rate-limiting step from enzymatic catalysis to physical mass transfer. This synergistic design extends the linear dynamic range by accurately controlling substrate flux and delaying enzyme kinetic saturation, thereby matching the sensing window to the requirements of hyperlactatemia monitoring. Through systematic optimization of AuNP deposition density, LOx-to-APTES ratio, and PVC membrane permeability, the sensor's linear range is extended to 0−60 mM, which fully covers the metabolic spectrum spanning physiological baseline levels to pathological hyperlactatemia (Figures S6 to S9).

To translate this high-performance sensing module into clinical practice, a fully integrated wearable platform is developed for noninvasive, real-time monitoring of hyperlactatemia (Figure 1f). The device features a multiplexed electrochemical sensing array, carbachol hydrogel-loaded electrodes for on-demand sweat induction, a biomimetic microfluidic layer for continuous sample refreshment, and a customized printed circuit board (PCB) for real-time signal processing (Figures 1g, S10 and S11). By incorporating lactate, pH, and temperature sensors, the system enables *in situ* signal monitoring and calibration, thereby preserving analytical accuracy in the complex physiological environment of the ICU. Ultimately, the wearable device can be comfortably affixed to a patient's wrist, providing a reliable, atraumatic tool for continuous monitoring of hyperlactatemia via dynamic sweat lactate tracking (Figure S12).

Characterization and Calibration of the Integrated Sensor Array

Figure 2a schematically depicts the hierarchical electron transduction mechanism of our rationally engineered lactate-sensing interface, optimized to achieve a wide linear detection range. In this cascade, lactate oxidation by LOx generates H_2O_2, whose reductive flux at the PB-mediated electrode dictates the magnitude of the resulting cathodic current, establishing a quantitative amperometric response proportional to lactate concentration (Figure S13). Cyclic voltammetry reveals a concentration-dependent reduction peak centered at 0 V (vs Ag/AgCl) (Figure S14), which is selected as the optimal working potential to maximize Faradaic current and the signal-to-noise ratio (SNR). Furthermore, to determine the sampling window that balances response kinetics and analytical precision, we systematically investigated the chronoamperometric responses over a lactate concentration range of 0−60 mM. Within the 90−100 s interval, the diffusion layer stabilizes and the current reaches a steady state, yielding a coefficient of variation (CV) of approximately 1%, SNR > 100, and R^2 of 0.990 (Figure S15). Using this optimized 100 s sampling window, the sensor exhibits a linear response to 0−60 mM lactate in phosphate-buffered saline (PBS), with a sensitivity of −0.203 μA cm^{-2} mM^{-1} and R^2 of 0.999 (Figures 2b and S16a). Compared with state-of-the-art lactate sensors reported in prior literature,[18,19,22−25,31−37] the present system achieves a favorable trade-off between low-concentration sensing capability and a broad dynamic range (Figure 2c and Table S1). The selectivity of this sensor is rigorously evaluated against common electroactive sweat constituents, including nontarget electrolytes and metabolites. At a 10 mM lactate baseline, the

https://doi.org/10.1021/acsnano.6c12805
ACS Nano 2026, 20, 28602−28616

Downloaded from pubs.acs.org/ancac3/article-pdf/20/42/28602/6882571/2/acsnano.6c12805.pdf by CITY UNIV OF HONG KONG user on 11 November 2026

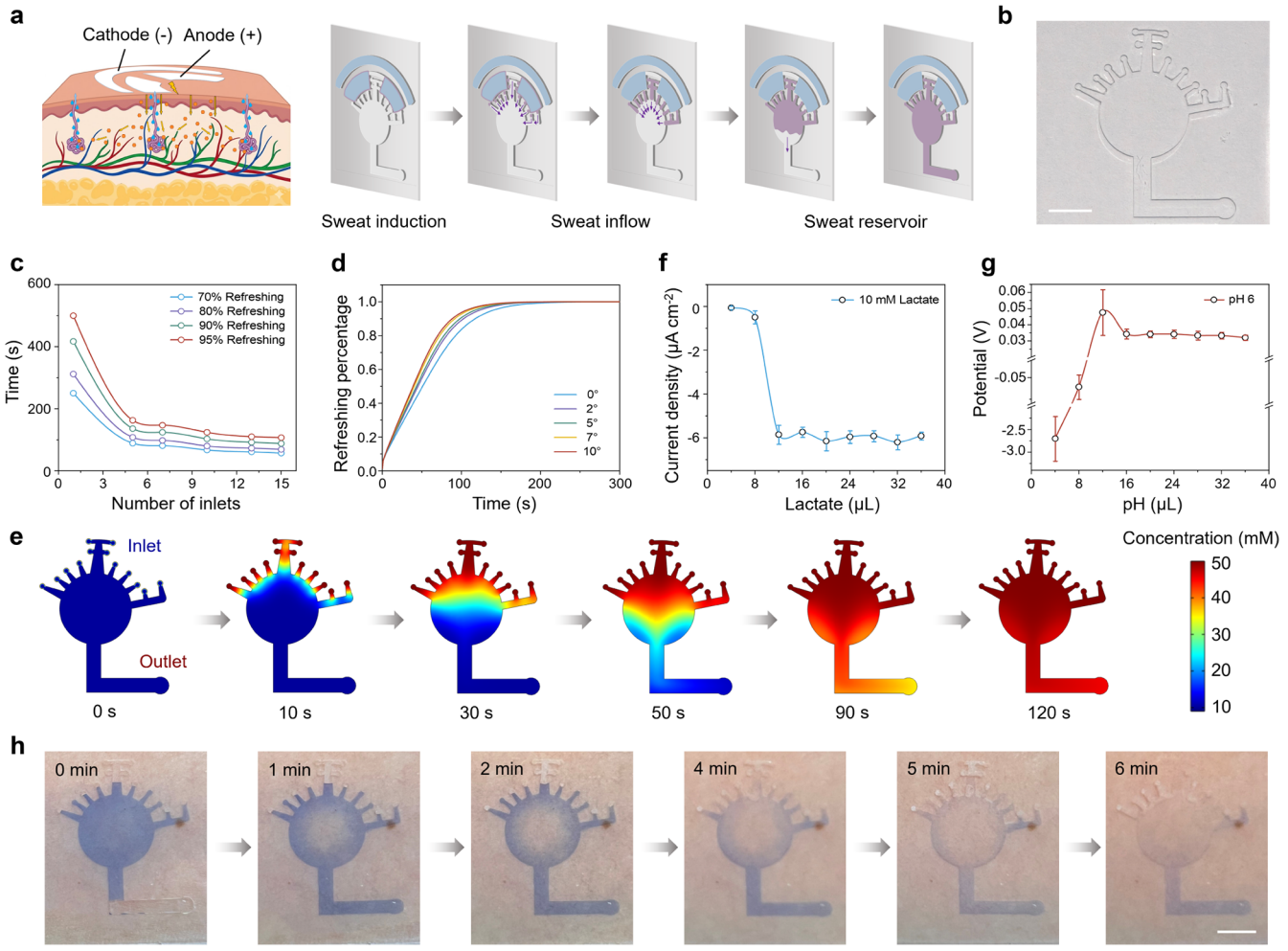


Figure 3. Fabrication and dynamic performance of the sweat microfluidic system. (a) Schematic illustration of the integrated microfluidic system enabling iontophoretic sweat induction, automated sampling, and fluid refreshment. (b) Optical image of the microfluidic patch. Scale bar, 5 mm. (c) Simulated dependence of refreshing time on inlet number within 10−50 mM. (d) Simulated dependence of refreshing percentage on channel wedge angle within 10−50 mM. (e) Numerically simulated spatial and temporal distributions of lactate concentration across the microfluidic network. Number of inlets, 13; flow rate of each inlet, 1.5 μL min^{-1}. (f) Current density response of the multiplexed lactate sensor to varying sample volumes. (g) OCP response of the multiplexed pH sensor to varying sample volumes. (h) On-body evaluation of the flexible microfluidic reservoir during carbachol-stimulated sweat secretion at rest. Scale bar, 5 mm. Error bars represent mean ± SD, n = 3.

device maintains high selectivity with negligible signal deviations within ± 5.5% (Figures 2d, S16b, and Table S2). Reproducibility assessments across 15 sensors from five independent batches show a relative standard deviation (RSD) of 3.015% at 10 mM lactate, which confirms exceptional intrabatch consistency and interbatch stability (Figure 2e). Additionally, the lactate sensor shows a current-density drift of 0.29 μA cm^{-2} over 6 h at 10 mM lactate, corresponding to an apparent change of 1.43 mM (Figure S17).

To minimize the resulting sensing bias and enable high-precision sweat lactate quantification, we integrate on-chip pH and temperature sensors for in situ calibration. The pH sensor is prepared by sequentially electrodepositing Poly(3,4-ethylenedioxythiophene):poly(styrenesulfonate) (PEDOT:PSS) and polyaniline (PANI) onto the LEG substrate (Note S5 and Figures S18, S19). As a high-performance solid-contact transducer, PEDOT:PSS reduces interfacial impedance and suppresses potential drift, ensuring stable potentiometric signal output.[38] PANI delivers pH-sensitive potentiometric responses, which originate from the reversible protonation and deprotonation of its imine nitrogen sites.[39] Based on open-circuit potential (OCP) data, the pH sensor displays a sensitivity of −51 mV pH^{-1} across the physiological range from pH 4.0 to 9.0, with an R^2 of 0.996 (Figures 2f and S20a). Subsequent cyclic testing among varied pH buffers further confirms excellent reversibility and fast temporal response (Figures 2g, S20b and S20c). Specificity evaluations verify robust anti-interference performance, as the potentiometric response remains stable within ±2 mV even under fluctuating thermal conditions and complex ionic backgrounds (Figures 2h and S20d). In dynamic real-time fluid tests using stirred PBS, it also maintains strong temporal consistency with readings from a commercial pH meter (Figure S20e). Moreover, 15 sensors from five independent batches yield an RSD of 0.319% at pH 6.0, confirming exceptional interbatch reproducibility (Figure S20f). Meanwhile, the pH sensor exhibits a 4.74 mV drift over 6 h at pH 5, equivalent to a pH error of 0.09 (Figure S21). To facilitate the evaluation of temperature-induced interference and subsequent calibration

https://doi.org/10.1021/acsnano.6c12805
ACS Nano 2026, 20, 28602−28616

Downloaded from pubs.acs.org/ancac3/article-pdf/20/42/28602/6882571 2/acsnano.6c12805.pdf by CITY UNIV OF HONG KONG user on 11 November 2026

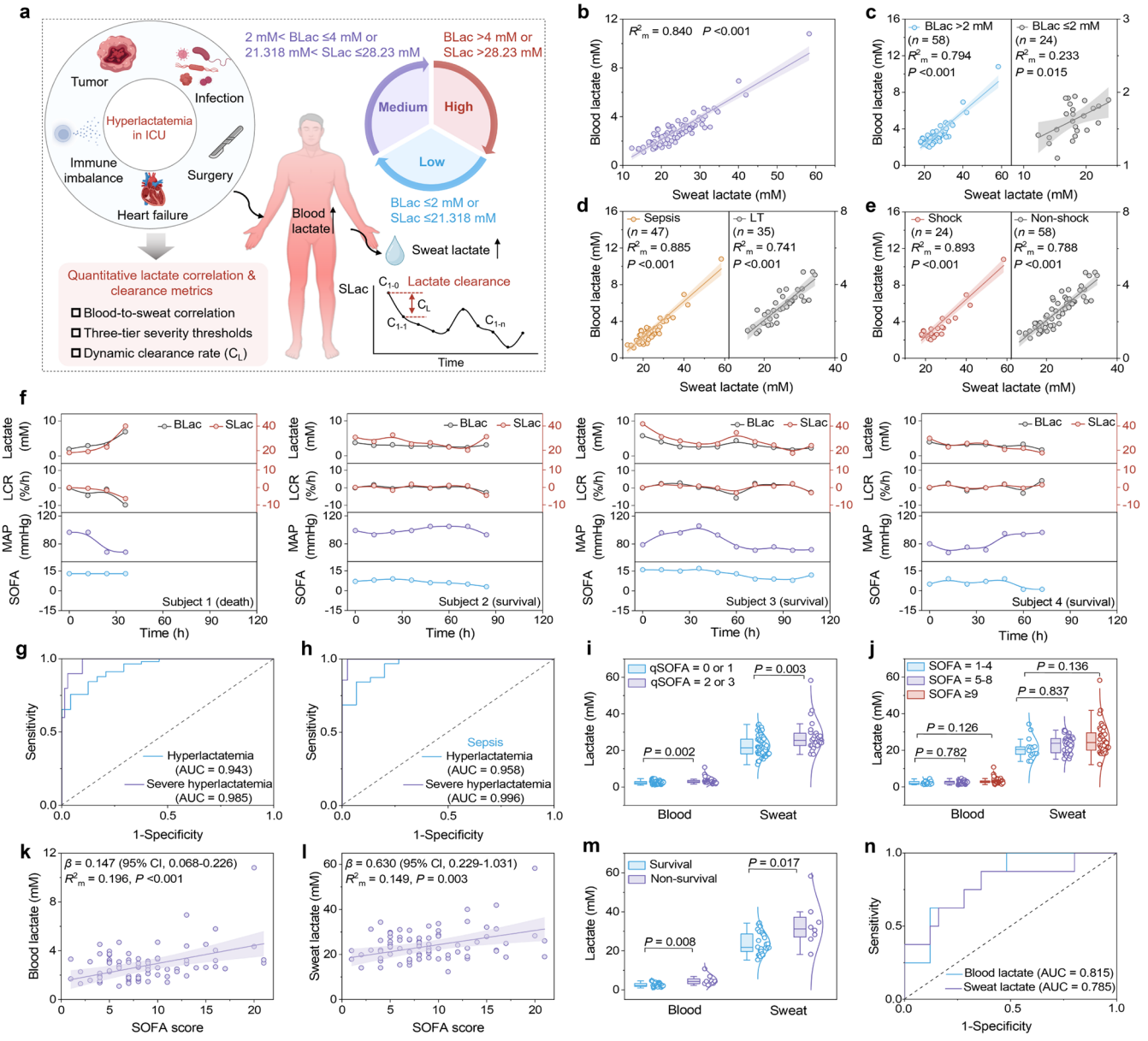


Figure 4. Clinical validation of sweat lactate as a biomarker in critically ill patients. (a) Clinical framework for continuous sweat lactate monitoring. (b to e) Mixed-effects associations between sweat and blood lactate in the overall cohort (b), stratified by hyperlactatemia (c), clinical conditions (sepsis vs LT) (d), and hemodynamic status (shock vs non-shock) (e). Each point represents one paired measurement. Lines and 95% CIs were derived from models with patient-specific random intercepts. (f) Representative physiological trajectories from four critically ill patients, comprising one nonsurvivor (Subject 1) and three survivors (Subjects 2 to 4). (g and h) Measurement-level ROC curves of sweat lactate for diagnosing hyperlactatemia and severe hyperlactatemia in the overall (g) and sepsis (h) cohorts. (i and j) Blood and sweat lactate stratified by qSOFA (i) and SOFA scores (j), with *P* values derived from mixed-effects models. (k and l) Mixed-effects associations between blood (k) and sweat (l) lactate levels with SOFA scores. (m) Lactate levels in survivors and non-survivors. (n) ROC curves of blood and sweat lactate for predicting in-hospital mortality. Panels m and n include one paired measurement per patient, selected at the highest recorded SOFA score. Lactate levels were measured using a colorimetric assay in paired sweat and blood specimens.

for lactate sensing, we further integrate a resistive temperature sensor into the same sensing array (Note S5). The LEG-based resistive temperature sensor delivers stable response behavior from 25 to 50 °C, with a sensitivity of −0.4 Ω °C^{-1} and an R^2 of 0.995 (Figures 2i and S22a). Additionally, reproducibility measurements performed on 15 sensors covering five independent batches reveal favorable reproducibility at 35 °C (Figure S22b).

To enable accurate quantification of lactate under physiological conditions, we systematically evaluated the influence of pH and temperature fluctuations on the response of the lactate sensor. As shown in Figure 2j and k, the lactate sensor shows exceptional robustness across a physiologically relevant pH range of 4.5 to 7.4, which is attributed to the protective microenvironment provided by the LOx/APTES matrix. Despite significant pH variations, the lactate sensor maintains a consistent linear detection range (0−60 mM) with sensitivities stabilized between −0.198 and −0.216 μA cm^{-2} mM^{-1} and R^2 > 0.95 (Figures S23 and S24). In contrast to pH variations, temperature exerts a pronounced regulatory effect on the lactate response. Between 25 and 45 °C, the current density of the lactate sensor demonstrates a robust linear

https://doi.org/10.1021/acsnano.6c12805
ACS Nano 2026, 20, 28602−28616

Downloaded from pubs.acs.org/ancac3/article-pdf/20/42/28602/6882571 2/acsnano.6c12805.pdf by CITY UNIV OF HONG KONG user on 11 November 2026

decrease with increasing temperature, a trend consistently observed at both 10 mM and 40 mM lactate levels (Figure 2l). The thermal coefficient remains independent of the lactate concentration, indicating a predictable interference pattern that can be readily corrected via calibration. Figure 2m presents the 3D response profiles at 10 mM lactate, highlighting the combined effects of coupled temperature and pH variations on the lactate sensor response. Consequently, by incorporating pH and temperature sensors, the lactate biosensor can perform real-time synchronous calibration and thereby afford high-precision sweat monitoring in diverse clinical scenarios.[40] Furthermore, to assess the electronic readout under an on-body operating configuration, the integrated sensor array was calibrated via the wearable PCB and benchmarked against an electrochemical workstation. PCB-derived lactate, pH, and temperature responses show stable plateaus, high repeatability, and calibration slopes consistent with benchtop measurements (Figure S25).

On-Demand Sweat Sampling Platform

To apply the calibrated high-fidelity sensor array in clinical critical care settings, reliable sweat sampling is an essential prerequisite for accurate, real-time, continuous sweat lactate monitoring. However, critically ill patients under deep sedation, anesthesia, or shock present pathological anhidrosis with no spontaneous sweating for consistent sampling and cannot undergo conventional exercise-induced sweat collection. To overcome these barriers, we developed an integrated platform comprising an IP module for on-demand sweat induction, paired with a hydrophilic microfluidic module for efficient sweat transport to the sensing reservoirs (Figure 3a,b and Note S6).

The IP module consists of LEG-based anodes and cathodes functionalized with carbachol-loaded hydrogels to locally stimulate sweat gland secretion in critically ill patients with anhidrosis, with the potential to trigger sustained and reproducible sweat responses.[41−43] Coupled with hydrophilic microchannels, the induced sweat is transported across the sensing chamber without external pumping. To minimize sampling latency, we performed finite element analysis to numerically optimize the microfluidic architecture and systematically evaluate the influence of inlets and the wedge angle of the flow channels on solute exchange efficiency (Figures S26 and S27). The simulation results demonstrate that the optimized design with 13 inlets and a 7° wedge angle allows over 95% of the chamber's solutes to be renewed within approximately 120 s under a 10−50 mM concentration step, ensuring near-real-time tracking of dynamic biomarkers (Figure 3c−e). Experimental assessments confirm that a microvolume of approximately 16 μL suffices to completely immerse the sensor array and form a stable electrochemical double layer, thereby ensuring robust potential stability and high-fidelity lactate detection without sacrificing temporal resolution (Figure 3f and g). Consistent with the simulated fluid dynamics, on-body trials confirm a 6 min refresh time, with preinjected blue ink fully cleared from the sensing area via microchannels to enable efficient sweat refreshment (Figure 3h). This seamless integration of autonomous iontophoretic induction and microfluidic sampling overcomes the inherent limitations of passive collection, delivering robust, real-time sweat lactate monitoring in critical care settings.

Clinical Validation of Sweat Lactate in Critically Ill Patients

Toward clinical translation of the integrated sweat-sensing platform in critical care, a prospective cohort study was performed to validate its utility as a noninvasive alternative to blood lactate analysis for ICU applications (Figure 4a). The cohort comprised 33 critically ill patients, who represented key clinical subgroups including sepsis, liver transplantation (LT), hyperlactatemia, shock, vasopressor support, and continuous renal replacement therapy (CRRT). Demographic, biochemical, and clinical outcome data are presented in Tables S3 and S4. From these participants, we systematically collected 82 paired sweat-blood samples. This data set was used to characterize the association between sweat and blood lactate and to validate whether sweat lactate offers prognostic equivalence relative to conventional blood-based monitoring. Within this clinical cohort, median blood lactate was 2.640 mM (IQR, 1.896−3.257 mM). By comparison, paired sweat lactate exhibited a median of 23.000 mM (IQR, 19.000−27.617 mM) and reached a maximum of 58.300 mM. Notably, the measured sweat lactate concentrations lie well within the sensor-calibrated working range of 0−60 mM, supporting its technical suitability for clinical monitoring.

Sweat lactate measurements exhibited a strong association with corresponding blood lactate levels, yielding R^2_m = 0.840 (β = 0.185, 95% CI, 0.169−0.200, P < 0.001) (Figure 4b and Table S5). According to the established sweat-to-blood mixed-effects model, predicted blood lactate values (BL_{pred}) are derived from sweat lactate levels. Subsequent Bland−Altman analysis confirms exceptional concordance between BL_{pred} and clinically determined blood lactate values (BL_{act}) (Figure S28). Importantly, this robust association remains consistent across all major clinical subgroups assessed, including hyperlactatemia (R^2_m = 0.794, Figure 4c), sepsis (R^2_m = 0.885, Figure 4d), LT (R^2_m = 0.741, Figure 4d), shock (R^2_m = 0.893, Figure 4e), CRRT (R^2_m = 0.839, Figure S29a), and vasopressor support (R^2_m = 0.888, Figure S29b). Longitudinal monitoring in four representative ICU patients further revealed close temporal correspondence between sweat and blood lactate profiles (Figure 4f). During episodes of acute hemodynamic instability, sweat lactate kinetics parallel those of blood lactate, permitting sensitive tracking of dynamic changes in tissue perfusion.

Given that hyperlactatemia (arterial lactate >2 mM) and severe hyperlactatemia (arterial lactate >4 mM) are closely associated with sepsis, multiple organ dysfunction syndrome, and in-hospital mortality,[44−46] the diagnostic efficacy of sweat lactate for hyperlactatemia was quantified using receiver operating characteristic (ROC) analysis. As illustrated in Figure 4g, sweat lactate accurately identified both hyperlactatemia and severe hyperlactatemia, with areas under the curve (AUCs) of 0.943 (95% CI, 0.871−0.982) and 0.985 (95% CI, 0.946−1.000), respectively. The optimal sweat cutoff values are determined to be 21.318 mM and 28.230 mM, with corresponding sensitivities of 0.845 and 1.000, and specificities of 0.875 and 0.903, respectively (Table S6). Subgroup analysis further confirms the robust diagnostic capacity of sweat lactate in sepsis and LT cohorts, with an AUC of more than 0.9 (Figures 4h and S30). These findings support the utility of sweat lactate as a noninvasive surrogate biomarker for clinical risk stratification and decision-making in critical care settings.

Furthermore, we assessed the clinical association between sweat lactate profiles and established clinical scoring systems, including the quick Sequential Organ Failure Assessment Score (qSOFA) and the Sequential Organ Failure Assessment Score

Downloaded from pubs.acs.org/ancac3/article-pdf/20/42/28602/6882571 2/acsnano.6c12805.pdf by CITY UNIV OF HONG KONG user on 11 November 2026

https://doi.org/10.1021/acsnano.6c12805
ACS Nano 2026, 20, 28602−28616

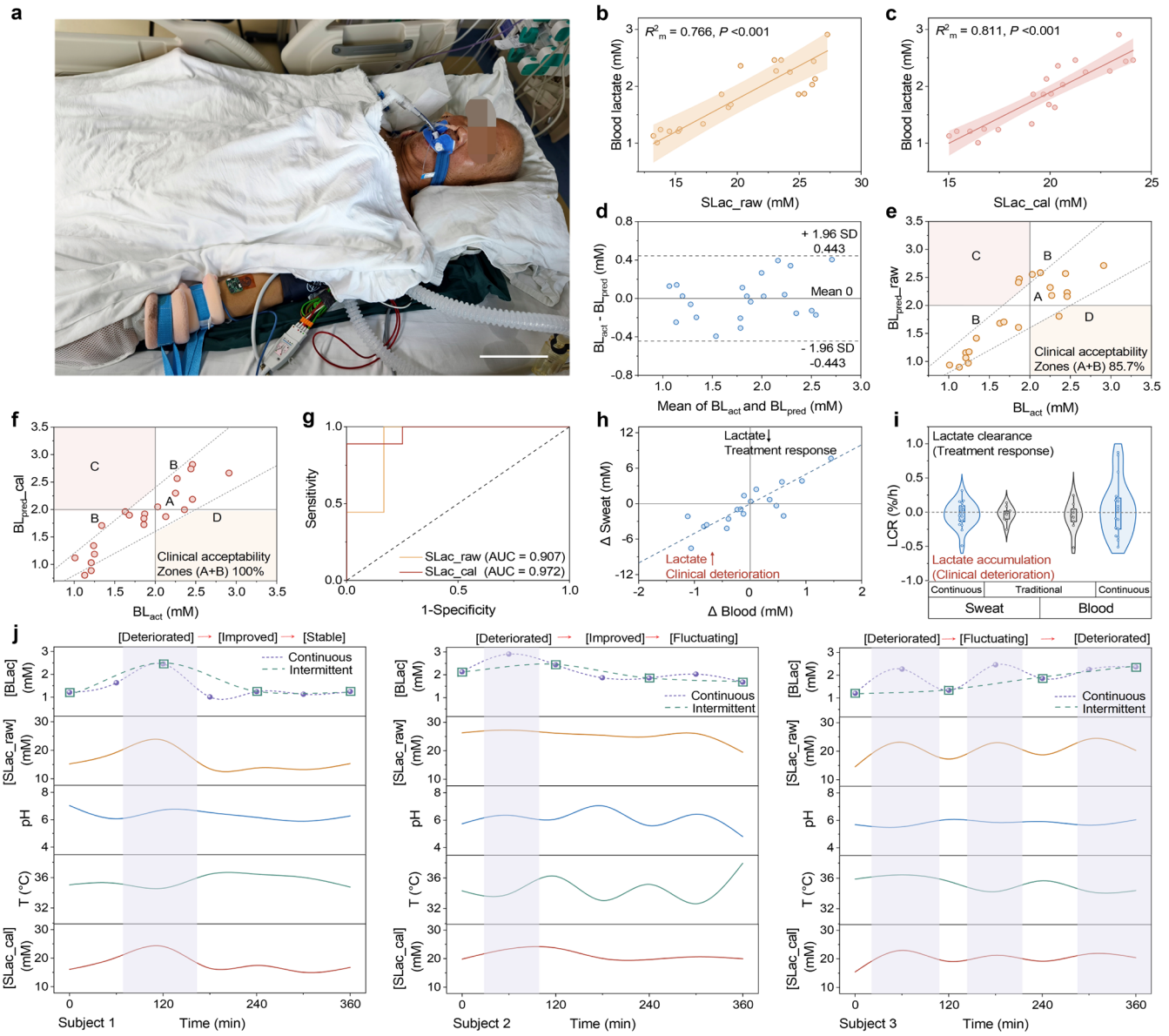


Figure 5. Feasibility of the wearable sweat lactate monitoring system in critically ill patients. (a) Photograph of a critically ill patient wearing the integrated wearable device. Scale bar, 10 cm. (b and c) Mixed-effects associations between ABG-measured blood lactate and device-measured sweat lactate before (b) and after (c) calibration. Each point represents one paired measurement. Lines and 95% CIs are from models with patient-specific random intercepts. (d) Bland−Altman analysis of mixed-model-predicted and ABG-measured blood lactate. (e and f) Clinical acceptability and error grid analysis before (e) and after (f) calibration. Dashed lines show ± 20% deviation and solid lines the 2 mM hyperlactatemia threshold. (g) Exploratory measurement-level ROC curves of sweat lactate for hyperlactatemia detection. (h) Concordance rate plot of device-measured sweat lactate versus paired blood lactate. Each point represents the 1 h change in paired sweat and blood lactate, calculated as $\Delta C = C_{t1} - C_{t2}$. (i) Lactate clearance rate and accumulation dynamics captured by continuous versus traditional intermittent sampling. The continuous and traditional intermittent series used consecutive 1 h intervals (0−1, 1−2, 2−3, 3−4, 4−5, and 5−6 h) and 2 h intervals (0−2, 2−4, and 4−6 h), respectively. (j) Representative continuous multiplexed monitoring profiles in three critically ill patients.

(SOFA).[47−50] Specifically, patients in the high-risk group (qSOFA = 2 or 3) exhibited significantly higher sweat lactate levels after adjustment for within-patient correlation (P = 0.003, Figure 4i). By contrast, categorical comparisons based on SOFA scores did not yield statistical significance in the mixed-effects analysis (Figure 4j). The qSOFA-driven stratification was particularly pronounced among the sepsis subgroup (Figure S31). We further performed mixed-effects analysis with continuous variables, which showed that the SOFA score is positively associated with both systemic blood lactate (β = 0.147, 95% CI, 0.068−0.226, P < 0.001) and sweat lactate (β = 0.630, 95% CI, 0.229−1.031, P = 0.003) (Figure 4k and l). This association remains significant within the sepsis subgroup, despite the complex pathophysiology in this cohort (blood: β = 0.176, 95% CI, 0.067−0.285, P = 0.002; sweat: β = 0.821, 95% CI, 0.290−1.352, P = 0.004) (Figure S32). Collectively, these results indicate that sweat lactate can serve as a continuous readout for tracking the clinical progression of critically ill patients. We next assessed the prognostic performance of sweat lactate using one paired measurement per patient, selected at each patient's maximum recorded SOFA score during the study period. Both blood and sweat

https://doi.org/10.1021/acsnano.6c12805
ACS Nano 2026, 20, 28602−28616

Downloaded from pubs.acs.org/ancac3/article-pdf/20/42/28602/6882571 2/acsnano.6c12805.pdf by CITY UNIV OF HONG KONG user on 11 November 2026

lactate concentrations were significantly higher in nonsurvivors than survivors, with P values of 0.008 and 0.017, respectively (Figure 4m). Sweat lactate demonstrates strong prognostic utility for in-hospital mortality (Figure 4n), with an AUC of 0.785, comparable to that of blood lactate analysis (AUC of 0.815). These observations highlight the potential of sweat lactate as a noninvasive prognostic biomarker for risk stratification in critical care settings.

Bedside Feasibility in Critically Ill Patients

Prior to clinical pilot study, we validated the performance of the wearable system using both artificial sweat and ex vivo human clinical sweat samples. Across a set of 15 artificial sweat specimens, sensor-derived lactate and pH readings showed close concordance with measurements from the reference colorimetric assay (r = 0.995, P < 0.001) and a pH meter (r = 0.997, P < 0.001), respectively (Figure S33). For sweat specimens collected from five critically ill patients, absolute relative errors spanned 0.9% to 5.4% for lactate and 0.3% to 0.7% for pH (Figure S34). We further performed paired comparisons of electrochemical responses between natural and iontophoresis-induced sweat from patients. Mean measurement errors remained below 3% for lactate and 1% for pH (Figure S35), indicating no appreciable stimulation-related measurement bias.

To evaluate the clinical applicability of this integrated biosensing device in high-acuity settings, we performed a pilot trial involving three critically ill patients (Figure 5a). The accuracy of the on-body lactate monitoring was validated by comparing sweat-sensing data with blood lactate values obtained from ABG analysis (mean blood lactate of 1.838 mM and a range of 1.010−2.910 mM). This wearable system has undergone formal clinical validation and obtained institutional certification from the First Affiliated Hospital of Xi'an Jiaotong University, verifying its safety and feasibility for ICU applications (see Clinical Translation Study Report for Medical Devices in Supporting Information). During 6-h longitudinal monitoring of the three enrolled patients, raw sweat-sensing profiles exhibit a strong association with blood lactate, with an R^2_m of 0.766 (Figure 5b). Notably, pH- and temperature-based calibration significantly strengthens the sweat−blood lactate association, yielding an improved R^2_m of 0.811 (Figure 5c). Bland−Altman analysis confirms superior consistency of calibrated measurements, with a mean bias of 0 mM (95% limits of agreement, −0.443 to 0.443 mM) (Figure 5d). Furthermore, multiparameter compensation effectively corrects aberrant metabolic trajectories to clinically acceptable ranges (overall 100%, Zone A: 85.7%, Zone B: 14.3%), thereby minimizing diagnostic biases and clinical risks induced by uncalibrated raw signals in complex ICU settings (Figure 5e and f). In this exploratory measurement-level ROC analysis, the AUC for hyperlactatemia detection was numerically higher following calibration relative to uncalibrated readings (0.972 vs 0.907, Figure 5g).

To assess the temporal fidelity of this integrated device in capturing dynamic lactate fluctuations, we analyzed the rate of change in paired sweat and blood measurements (Figure 5h). Results indicate that sweat lactate trends closely mirror blood lactate trends with a concordance rate of 83%. The 2026 Surviving Sepsis Campaign (SSC) guidelines recommend serial lactate measurements every 2−4 h in patients with sepsis-induced hyperlactatemia.[8] We compared traditional intermittent blood sampling (every 2 h) with our continuous monitoring approach to simulate this standard-of-care protocol. Evidently, intermittent blood sampling fails to capture hyperacute metabolic fluctuations, restricting data capture and masking true lactate kinetics (Figure 5i). Accordingly, we propose a combined clinical paradigm that integrates intermittent gold-standard ABG measurements with real-time sweat lactate monitoring. Within this framework, periodic ABG testing provides definitive diagnostic accuracy, while the wearable system captures the full temporal profile of lactate clearance. By bridging the monitoring gaps inherent to discrete blood sampling, this dual-modal strategy may reduce potential clinical risks, such as missed diagnoses and delayed interventions, under dynamically changing ICU conditions.

Building on the validated accuracy and dynamic tracking capability of our integrated sensing platform, Figure 5j illustrates continuous multimodal monitoring profiles from the three ICU patients over a 6-h observation period. The sensing system demonstrates high sensitivity to dynamic fluctuations in the patient's metabolic status. Specifically, during episodes of clinical deterioration, sweat lactate levels increased in synchrony with increases in blood lactate. In contrast, both biomarkers exhibited parallel decreasing trends during clinical stabilization or favorable therapeutic responses. The system also reliably captured dynamic variations in the local skin temperature and sweat pH over the monitoring interval. Acquisition of these comprehensive multimodal data sets establishes an essential foundation for accurate in situ biochemical calibration and longitudinal clinical assessment. Furthermore, no adverse events such as erythema, pruritus, or secondary skin infections were observed at the sensor application sites throughout the trial, supporting the safety and tolerability of the wearable platform for prolonged critical-care monitoring.

CONCLUSIONS

Our integrated biosensing system represents a transformative advance toward real-time, self-calibrated surveillance of hyperlactatemia in critically ill patients. Through rational engineering of a LEG-AuNP conductive substrate and an APTES/LOx-PVC dual-diffusion-limiting sensing interface, the lactate sensor achieves an extended linear detection range of 0−60 mM by enhancing the electroactive surface area and mitigating enzyme saturation. This broad sensing range supports the reliable capture of pathological lactate surges of severe hyperlactatemia in critical illness. By integrating pH and temperature calibration modules in the same array, together with a microfluidic system and a data processing circuit, the platform enables fully automated high-precision lactate monitoring. Beyond engineering innovation, our clinical cohort study establishes robust physiological relevance between sweat and blood lactate and validates sweat lactate as a reliable metabolic proxy for identifying hyperlactatemia, stratifying disease severity, and predicting in-hospital mortality. Furthermore, the device demonstrates excellent temporal alignment with gold-standard ABG analysis during continuous bedside monitoring in the ICU. Together, these findings highlight the strong translational potential of this platform as a noninvasive alternative to conventional intermittent blood sampling for critical-care monitoring.

Downloaded from pubs.acs.org/ancac3/article-pdf/20/42/28602/6882571 2/acsnano.6c12805.pdf by CITY UNIV OF HONG KONG user on 11 November 2026

https://doi.org/10.1021/acsnano.6c12805
ACS Nano 2026, 20, 28602−28616

METHODS

Materials

Agarose, bovine serum albumin (BSA), hydrogen tetrachloroaurate-(III), PVC, DOS, APTES, iron(III) chloride ($FeCl_3$), potassium hexacyanoferrate(III) [$K_3Fe(CN)_6$], lactate, Nafion 117 solution, 3,4-Ethylenedioxythiophene (EDOT), poly(sodium 4-styrenesulfonate) (NaPSS), potassium chloride (KCl), sodium chloride (NaCl), anhydrous calcium chloride ($CaCl_2$), magnesium chloride ($MgCl_2$), anhydrous dextrose (D-glucose) (GLU), uric acid (UA), ascorbic acid (AA), urea, sodium hydroxide (NaOH), ammonium chloride (NH_4Cl), and aniline were obtained from Shanghai Aladdin Biochemical Technology Co., Ltd. (China). Carbachol was purchased from Sigma-Aldrich. Hydrochloric acid, acetic acid, THF, isopropyl alcohol, and PBS were obtained from Thermo Fisher Scientific. Lactate oxidase (106 U mg^{-1}) was purchased from Toyobo Co. The polydimethylsiloxane (PDMS) prepolymer was prepared using a silicone elastomer kit (Sylgard 184, Dow Corning, USA) by mixing the base monomer and curing agent at a 10:1 (w/w) ratio. PI films (0.125 mm in thickness) were purchased from DuPont. A wearable sweat inducer (HELA-SWI-007) was purchased from Ziqishun Biotechnology Co., Ltd. (Nanjing, China). An L-Lactic Acid (LA) Colorimetric Assay Kit (Elabscience, Wuhan, China) was used for lactate quantification.

Fabrication of the Sensor Patch

A PI film was raster-engraved at a specified focus height to fabricate LEG-based IP electrodes, connection leads, dedicated working electrodes for pH, temperature, and lactate detection, as well as shared counter and reference electrodes using a 50 W CO_2 laser cutter (Universal Laser System). The shared Ag/AgCl reference electrode was fabricated by uniformly drop-casting conductive silver paste onto the LEG electrode. Then, the electrode was modified by drop-casting a 10-μL aliquot of 0.1 M $FeCl_3$ for 1 min to form a stable Ag/AgCl reference interface. The pH sensor was prepared by first electrochemically cleaning the LEG electrode in 0.5 M HCl via cyclic voltammetry over a potential range of −0.1 to 0.9 V at a scan rate of 0.1 V s^{-1} for five cycles under ambient conditions. To mitigate potential drift, a PEDOT:PSS layer was then deposited by applying multicurrent-step polarization (8×10^{-6} A) for 900 s in a freshly prepared solution containing 0.01 M EDOT and 0.1 M NaPSS. The electrodes were then electrodeposited with a polyaniline pH-sensing membrane via cyclic voltammetry over a potential range of −0.2 to 1.0 V at 0.1 V s^{-1} for 30 cycles in a freshly prepared solution containing 0.1 M aniline and 1 M HCl to ensure uniform membrane formation.

The lactate sensor was fabricated using the same electrochemical cleaning protocol on the LEG electrode as described above. Subsequently, AuNPs were electrodeposited onto the carbon surface of the LEG electrode using pulsed voltammetry (0.3 to −1.1 V, 3000 cycles, 50 Hz) in a 50 mM $HAuCl_4$ solution to increase the electroactive surface area and sensing sensitivity. A PB transducer layer was then electrodeposited by cyclic voltammetry (4 cycles, −0.5 to 0.6 V, 50 mV s^{-1}) in a freshly prepared solution consisting of 2.5 mM $FeCl_3$, 2.5 mM $K_3Fe(CN)_6$, 100 mM KCl, and 100 mM HCl. To improve long-term stability, a NiHCF protective layer was further deposited by cyclic voltammetry (50 cycles, 0 to 0.8 V, 100 mV s^{-1}) in a solution of 0.5 mM $NiCl_2$, 0.5 mM $K_3Fe(CN)_6$, 100 mM KCl, and 100 mM HCl. The electrodes were then dried before drop-casting with the enzyme cocktail. This cocktail was prepared by mixing LOx (10 mg mL^{-1} in PBS) and APTES (1.5% in isopropanol) at a 3:7 (v/v) ratio. A 0.6 μL aliquot of enzyme cocktail was drop-cast onto the surface of each enzymatic sensor electrode and dried overnight at 4 °C. Finally, a diffusion-limiting membrane was further deposited by drop-casting 1.5 μL of a solution composed of 17 mg PVC and 65 mg DOS dissolved in 660 μL THF.

Structural Analysis and Electrochemical Evaluation of Sensors

The cross-sectional architecture of the LEG sensors was characterized using scanning electron microscopy (SEM), energy-dispersive X-ray spectroscopy (EDS), Raman spectroscopy, and X-ray photoelectron spectroscopy (XPS). Electrochemical characterization in vitro was performed using a CHI660E electrochemical workstation, with all analyte solutions prepared in 0.01 M PBS. To identify the optimal detection time window, amperometric curves, CV responses, and SNR values were calculated from the average current every 10 s over a 120-s duration. Furthermore, the coefficient of determination (R^2) for the linear fitting of lactate concentrations (0−60 mM) was analyzed across different time intervals to guarantee the optimal sensing reliability. Calibration of the pH sensor was conducted over a pH range of 4.0 to 9.0 using OCP measurements. The temperature sensor was characterized via resistive readout. A constant bias voltage of 1 V was applied across the LEG element, with the resulting current recorded and the resistance calculated according to Ohm's law ($R = V/I$). Temperature values were subsequently derived from the linear resistance−temperature calibration curve. For temperature characterization, ambient temperature was regulated from 25 to 50 °C using a ceramic heating plate. The 6 h stability of the lactate and pH sensors was evaluated independently using the integrated sensor array and a shared Ag/AgCl reference electrode. The artificial sweat solution consisted of 60 mM NaCl, 6 mM KCl, 5 mM NH_4Cl, 0.08 mM $MgCl_2$, 2.6 mM $NaHCO_3$, and 0.04 mM Na_2HPO_4. This base solution was adjusted to pH 6.5 using 0.1 M HCl. For pH-stability testing, an additional aliquot of this base solution was further adjusted to pH 5.0.

Microfluidic Modeling, Fabrication, and Evaluation

Fluid dynamics and analyte transport within the microchannels were simulated using COMSOL Multiphysics 5.6. Two-dimensional geometries of microfluidic devices were created in AutoCAD, imported into COMSOL, and modeled via coupling incompressible laminar flow with the Transport of Diluted Species module. The physical behavior was governed by the numerical solution of the Navier−Stokes equations for momentum conservation and the convection-diffusion equation for mass transport. A volumetric flow rate of 1.5 μL min^{-1} was imposed at the inlet, with no-slip boundary conditions imposed on all microchannel walls. Transient responses were evaluated by stepping the lactate concentration from 10 mM to 50 mM to mimic the physiological lactate fluctuations. Microfluidic channels were fabricated via photolithography and PDMS replica molding, using a silicon master with 200 μm-deep channels patterned with SU-8 photoresist. Before bonding and encapsulation, microfluidic chips were treated with oxygen plasma to hydroxylate their surfaces, ensuring robust sealing and efficient fluid loading. On-body fluid flow tests were performed to assess sweat transport efficiency within the microfluidic channels. An assembled microfluidic patch preloaded with blue dye in the sweat reservoir was attached to the forearm of a healthy subject, followed by in situ sweat induction via IP stimulation. Following the integration of microfluidic channels with composite electrode arrays, the minimum sample volume required for stable lactate and pH detection was quantified.

Fabrication of Sweat-Stimulating Hydrogels

Anodic and cathodic iontophoresis hydrogels were prepared using 4% (w/w) agarose. Agarose was dispersed in deionized water and heated with continuous stirring until fully dissolved. The resulting clear solution was removed from the heat source and allowed to cool while maintaining a fluid state. Carbachol (2% w/w) and NaCl (2% w/w) were subsequently added to the anodic and cathodic formulations, respectively. Following thorough mixing, the hydrogel formulations were cast into custom-fabricated PDMS molds and held at 4 °C until complete gelation. The finished hydrogels were stored at 4 °C prior to use.

Downloaded from pubs.acs.org/ancac3/article-pdf/20/42/28602/6882571 2/acsnano.6c12805.pdf by CITY UNIV OF HONG KONG user on 11 November 2026

https://doi.org/10.1021/acsnano.6c12805
ACS Nano 2026, 20, 28602−28616

Design of the Integrated PCB System

The PCB system integrated power management, wireless data processing, and electrochemical instrumentation modules. The power management unit utilized a rechargeable lithium battery with a voltage regulator providing a stable power supply for system operation. A dedicated boost converter provided a maximum compliance voltage of 36 V to the feedback-controlled current source. During iontophoresis, the circuit automatically adjusted the electrode voltage in response to variations in skin-electrode impedance and maintained a constant current of 1.5 mA over a 5 min stimulation period. Data processing and wireless communication connectivity were governed by a system-on-chip MCU with integrated Wi-Fi and an embedded electrochemical web server for remote data access. The MCU adopted an onboard ADC and DAC for high-precision signal acquisition and control. Electrochemical measurements were facilitated by a dedicated analog front-end (AFE), the LMP91000, which integrated a TIA and a control amplifier. Coupled with external voltage buffers, this AFE established a standard three-electrode configuration and completed signal conditioning for integrated pH, temperature, and lactate sensors.

For PCB-based calibration, the integrated sensor array was connected directly to the wearable circuit. Lactate current was recorded at 0 V versus the on-chip Ag/AgCl reference across 0−60 mM. pH responses were acquired via open-circuit potentiometry over pH 4.0−9.0, and temperature was derived from resistance measured under a 1 V bias across 25−50 °C. Steady-state calibration slopes were compared against those acquired using a benchtop electrochemical workstation.

Clinical Cohort Validation of Sweat−Blood Lactate Correlation

This prospective cohort study was conducted in the Surgical Intensive Care Unit of the First Affiliated Hospital of Xi'an Jiaotong University, with the protocol formally approved by the hospital's Institutional Review Board (XJTU1AF2024LSYY-522). Written informed consent was obtained from all participants or their legal representatives before study enrollment. Patients were recruited based on the following inclusion criteria: (i) age >18 years old; (ii) initial blood lactate >1.5 mM; (iii) baseline SOFA score >2; (iv) relatively stable hemodynamics (or hemodynamic stability achieved via pharmacological intervention) during the sampling period, ensuring tolerance to the necessary collection procedures. The exclusion criteria were considered as follows: (i) pregnancy; (ii) recent administration of high-dose anticholinergic agents or other drugs that interfered with sweat secretion; (iii) severe skin ulcers, inflammation, or severe edema that impaired sweat collection; and (iv) documented allergic reactions to device materials, such as PDMS and hydrogels. To guarantee standardized sampling and reduce systematic bias, an analytical instrument was utilized for controlled sweat stimulation and collection, with all procedures strictly synchronized with venous or arterial blood acquisition. Sweat−blood paired specimens were assayed for lactate concentration using a colorimetric kit. At each sampling point, mean arterial pressure (MAP) was captured via continuous bedside hemodynamic monitoring, SOFA and qSOFA scores were calculated from contemporaneous clinical and laboratory variables, while additional vital-sign readings and ABG-derived metabolic parameters were retrieved from routine clinical assessments.

Analytical Validation of the Wearable Sensor System

Analytical validation of the wearable sensor system was performed using both artificial and clinical human sweat samples. Fifteen artificial sweat samples with varied lactate and pH levels were measured using the wearable sensor platform. These identical samples were further analyzed using a reference colorimetric assay for lactate and a benchtop pH meter for pH. Subsequent clinical validation was conducted using sweat specimens collected from five critically ill patients, with each sample measured by both the wearable sensor and standard reference approaches for comparative analysis. Additionally, the potential influence of the complete sweat stimulation protocol on sensor readouts was independently evaluated in five critically ill patients using a paired-arm experimental design. Specifically, one forearm received carbachol iontophoresis at a current of 1.5 mA for 5 min to induce stimulated sweat production, whereas natural sweat was collected from the contralateral unstimulated forearm as the control. Under both stimulated and natural sweat conditions, steady-state lactate current density and pH open-circuit potential were continuously recorded. The absolute relative error was calculated as $|S_{IP} - S_{natural}|/|S_{natural}| \times 100\%$, where S represents the steady-state current density or open-circuit potential acquired from sensor detection.

On-Body Device Evaluation in Critically Ill Patients

The on-body clinical evaluation was performed in the Surgical Intensive Care Unit at the First Affiliated Hospital of Xi'an Jiaotong University. All three critically ill patients received their routine clinical treatment during sample collection. The volar forearm was defined as the unified measurement site to guarantee consistent sweat acquisition. During the 6 h bedside study, sweat was induced at baseline and hourly thereafter through 6 h. At each time point, a constant current of 1.5 mA was applied for 5 min to iontophoretically deliver carbachol. Sweat induction and electrochemical sensing were performed sequentially. The iontophoretic current was switched off before electrochemical acquisition, which began after fresh sweat had entered and refreshed the sensing chamber, and the sensor response had stabilized. Sweat lactate concentration was calculated from the steady-state current recorded between 90 and 100 s. Electrochemical signals were collected by the onboard circuit and transmitted through Wi-Fi to a mobile terminal or web server. At the corresponding time point, an arterial blood sample was drawn from the indwelling catheter and immediately analyzed using a clinical blood gas analyzer as the reference method. LCR from t1 to t2 was calculated as $(C_{t1} - C_{t2})/C_{t1} \times 100\%$, where C_{t1} and C_{t2} represent the lactate concentrations at the beginning and end of each 1-h or 2-h interval.

Statistical Analysis

All experiments were conducted in at least triplicate unless otherwise noted in the corresponding figure legends. Data normality was examined via the Shapiro−Wilk test. Given that most data sets exhibited non-normal distributions, nonparametric tests were adopted for group comparisons. Continuous clinical variables were expressed as medians with interquartile ranges. Between-group differences for non-normally distributed continuous variables were assessed using the Mann−Whitney U test for two independent groups and the Kruskal−Wallis H test for comparisons among three or more subgroups. Pairwise post hoc comparisons were performed using Dunn's test with Bonferroni correction for multiple comparisons.

Repeated clinical measurements were analyzed using linear mixed-effects models incorporating a patient-specific random intercept. Sweat lactate was set as the fixed-effect variable and patient identity as the random intercept for evaluating the physiological association between sweat and blood lactate concentrations. Fixed-effect slopes (β), 95% confidence intervals (95% CIs), marginal and conditional R^2 values, and intraclass correlation coefficients (ICCs) were reported. Bland−Altman analysis was applied to evaluate the agreement between predicted and measured blood lactate values. ROC curves were constructed to quantify the diagnostic performance of sweat lactate for hyperlactatemia and severe hyperlactatemia based on the AUC, sensitivity, and specificity. The optimal clinical cutoff was determined using Youden's index. To account for repeated measurements, 95% CIs for ROC parameters were estimated using patient-level cluster bootstrap resampling. For categorical fixed effects with >2 levels, pairwise contrasts of estimated marginal means were adjusted via the Tukey method. Group-level comparisons across qSOFA/SOFA strata and continuous associations between lactate concentrations and SOFA scores were assessed using random-intercept linear mixed-effects models. For mortality-related analyses, one paired measurement per patient was selected at the highest recorded SOFA score during the study period. All statistical tests were two-tailed, and $P < 0.05$ was defined as the threshold for statistical significance.

Downloaded from pubs.acs.org/ancac3/article-pdf/20/42/28602/6882571 2/acsnano.6c12805.pdf by CITY UNIV OF HONG KONG user on 11 November 2026

https://doi.org/10.1021/acsnano.6c12805
ACS Nano 2026, 20, 28602−28616

■ ASSOCIATED CONTENT

Data Availability Statement

The data that support the findings of this study are available in the Supporting Information of this article.

Supporting Information

The Supporting Information is available free of charge at https://pubs.acs.org/doi/10.1021/acsnano.6c12805.

Supporting notes: Clinical relevance and pathophysiology of hyperlactatemia in sepsis and critical illness; clinical implications of hyperlactatemia in perioperative liver transplantation; evaluating modalities for hyperlactatemia monitoring; biochemical and interfacial sensing mechanism of APTES-immobilized LOx lactate biosensors; working mechanisms of integrated pH and temperature sensors; design and analysis of the automated microfluidic system; Supporting figures: Pathophysiology and clinical impact of hyperlactatemia in critical illness; characterizations of LEG-AuNP nanostructures; Raman spectrum of LEG; XPS analysis of LEG; microscopic and elemental characterization of LEG-AuNPs-PB-NiHCF nanostructures; evaluation of the AuNPs layer for lactate sensing; evaluation of the cross-linked enzyme layer for lactate sensing; sensitivity of the integrated sensor across different LOx/APTES groups; evaluation of the diffusion-limit layer for lactate sensing; schematic illustration of the epidermal sensing patch fabrication process; circuit diagram of the sensing platform; wearable arm-attached sensing system for critically ill patient surveillance; electrochemical modification of the lactate electrode; representative cyclic voltammetry responses of the lactate sensor in PBS; chronoamperometric transient dynamics under varying lactate concentrations; electrochemical characterization of the lactate electrode; six-hour stability of the lactate sensor using the shared Ag/AgCl reference electrode in artificial sweat; schematic of the layered pH sensor architecture; electrochemical modification of the pH electrode; electrochemical characterization of the pH electrode; six-hour stability of the pH sensor using the shared Ag/AgCl reference electrode in artificial sweat; electrochemical characterization of the temperature sensing electrode; pH-dependent chronoamperometric response of the integrated lactate sensor; linear calibration plots for lactate detection under different pH conditions; end-to-end calibration of the integrated sensor array using the wearable PCB; numerical simulation of microfluidic patterns with varying inlet numbers; numerical simulation of microfluidic patterns with varying wedge angles; repeated-measures Bland–Altman plot assessing the clinical concordance of sweat and blood lactate levels; subgroup analysis of sweat-blood lactate associations; subgroup analysis of ROC curves for sweat lactate-based hyperlactatemia diagnosis; comparison of blood and sweat lactate levels stratified by clinical severity scores; association between lactate levels and SOFA scores; agreement between wearable-sensor and reference measurements in artificial sweat; direct validation of the wearable sensor in clinical sweat; paired comparison of electrochemical responses in natural and iontophoresis-induced sweat from critically ill patients; Supporting tables: Analytical comparison of our work and other sweat lactate sensors; selectivity of the lactate electrode against various interferences; demographics and clinical characteristics of study participants; laboratory parameters and disease severity for each sample; linear mixed-effects model analyses of sweat-blood lactate associations; ROC analysis for diagnosing hyperlactatemia based on sweat lactate; Clinical Translation Study Report for Medical Devices (PDF)

■ AUTHOR INFORMATION

Corresponding Authors

Kai Qu − *Department of Hepatobiliary Surgery and Liver Transplantation, The Second Affiliated Hospital of Xi'an Jiaotong University, Xi'an 710061, China; Key Laboratory of Surgical Critical Care and Life Support, Ministry of Education, Xi'an Jiaotong University, Xi'an 710049, China*; Email: qukai001@xjtu.edu.cn

Yunsheng Fang − *Department of Surgical ICU, The First Affiliated Hospital of Xi'an Jiaotong University, Xi'an 710061, China; The Key Laboratory of Biomedical Information Engineering of Ministry of Education, School of Life Science and Technology and Bioinspired Engineering & Biomechanics Center (BEBC), Xi'an Jiaotong University, Xi'an 710049, China*; orcid.org/0000-0003-2213-0167; Email: ysfang@xjtu.edu.cn

Yu Song − *Department of Biomedical Engineering, City University of Hong Kong, Hong Kong 999077, China*; orcid.org/0000-0002-4185-2256; Email: yusong@cityu.edu.hk

Ting Lin − *Department of Surgical ICU, The First Affiliated Hospital of Xi'an Jiaotong University, Xi'an 710061, China; Key Laboratory of Surgical Critical Care and Life Support, Ministry of Education, Xi'an Jiaotong University, Xi'an 710049, China*; Email: linda_ting@xjtufh.edu.cn

Authors

Yunxiang Long − *Department of Surgical ICU, The First Affiliated Hospital of Xi'an Jiaotong University, Xi'an 710061, China; Department of Hepatobiliary Surgery and Liver Transplantation, The Second Affiliated Hospital of Xi'an Jiaotong University, Xi'an 710061, China; The Key Laboratory of Biomedical Information Engineering of Ministry of Education, School of Life Science and Technology, Bioinspired Engineering & Biomechanics Center (BEBC), and Key Laboratory of Surgical Critical Care and Life Support, Ministry of Education, Xi'an Jiaotong University, Xi'an 710049, China*

Xiaosen Pan − *The Key Laboratory of Biomedical Information Engineering of Ministry of Education, School of Life Science and Technology and Bioinspired Engineering & Biomechanics Center (BEBC), Xi'an Jiaotong University, Xi'an 710049, China*; orcid.org/0000-0002-2760-4598

Yao Chen − *Department of Hepatobiliary Surgery and Liver Transplantation, The Second Affiliated Hospital of Xi'an Jiaotong University, Xi'an 710061, China; The Key Laboratory of Biomedical Information Engineering of Ministry of Education, School of Life Science and Technology and Bioinspired Engineering & Biomechanics Center (BEBC), Xi'an Jiaotong University, Xi'an 710049, China*

Nanpei Li − *The Key Laboratory of Biomedical Information Engineering of Ministry of Education, School of Life Science and Technology and Bioinspired Engineering & Biomechanics*

Downloaded from pubs.acs.org/ancac3/article-pdf/20/42/28602/6882571/2/acsnano.6c12805.pdf by CITY UNIV OF HONG KONG user on 11 November 2026

Center (BEBC), Xi'an Jiaotong University, Xi'an 710049, China

Wentong Wang − *The Key Laboratory of Biomedical Information Engineering of Ministry of Education, School of Life Science and Technology and Bioinspired Engineering & Biomechanics Center (BEBC), Xi'an Jiaotong University, Xi'an 710049, China*

Yuqi Wang − *Department of Biomedical Engineering, City University of Hong Kong, Hong Kong 999077, China;* orcid.org/0009-0009-4576-4219

Wanyu Zhang − *Department of Biomedical Engineering, City University of Hong Kong, Hong Kong 999077, China*

Taozhe Liu − *The Key Laboratory of Biomedical Information Engineering of Ministry of Education, School of Life Science and Technology and Bioinspired Engineering & Biomechanics Center (BEBC), Xi'an Jiaotong University, Xi'an 710049, China*

Qiuting Peng − *Department of Surgical ICU, The First Affiliated Hospital of Xi'an Jiaotong University, Xi'an 710061, China; Department of Hepatobiliary Surgery and Liver Transplantation, The Second Affiliated Hospital of Xi'an Jiaotong University, Xi'an 710061, China; Key Laboratory of Surgical Critical Care and Life Support, Ministry of Education, Xi'an Jiaotong University, Xi'an 710049, China*

Kun Yang − *Department of Surgical ICU, The First Affiliated Hospital of Xi'an Jiaotong University, Xi'an 710061, China; Department of Hepatobiliary Surgery and Liver Transplantation, The Second Affiliated Hospital of Xi'an Jiaotong University, Xi'an 710061, China; Key Laboratory of Surgical Critical Care and Life Support, Ministry of Education and School of Future Technology, Xi'an Jiaotong University, Xi'an 710049, China*

Guorui Jin − *The Key Laboratory of Biomedical Information Engineering of Ministry of Education, School of Life Science and Technology and Bioinspired Engineering & Biomechanics Center (BEBC), Xi'an Jiaotong University, Xi'an 710049, China;* orcid.org/0009-0000-9775-0374

Chang Liu − *Department of Hepatobiliary Surgery and Liver Transplantation, The Second Affiliated Hospital of Xi'an Jiaotong University, Xi'an 710061, China; Key Laboratory of Surgical Critical Care and Life Support, Ministry of Education, Xi'an Jiaotong University, Xi'an 710049, China*

Jian Lv − *Frontier Institute of Science and Technology (FIST), Xi'an Jiaotong University, Xi'an 710049, China;* orcid.org/0000-0003-3425-2882

Feng Xu − *The Key Laboratory of Biomedical Information Engineering of Ministry of Education, School of Life Science and Technology and Bioinspired Engineering & Biomechanics Center (BEBC), Xi'an Jiaotong University, Xi'an 710049, China*

Complete contact information is available at: https://pubs.acs.org/10.1021/acsnano.6c12805

Author Contributions

◆Y.L. and X.P. contributed equally to this work. Y.L., Y.F., and T.L. conceived the project. Y.L., C.L., T.L., K.Q., Y.S., F.X., and Y.F. supervised the research. Y.L., T.L., C.L., K.Q., F.X., and Y.F. designed the research. Y.L., K.Y., and X.P. developed and characterized the lactate, temperature, and pH sensors. J.L., Y.L., and Y.C. performed FEA simulations and characterization of the sweat microfluidic channel. Y.L., X.P., and N.L. developed and evaluated the PCB. W.W., Y.W., W.Z., Y.L., K.Y., and Q.P. assisted in the collection of paired blood and sweat samples and the ICU testing of the integrated device. Y.L. and X.P. performed statistical analysis. Y.L., X.P., Y.C., Q.P., N.L., G.J., K.Q., T.L., Y.S., and Y.F. wrote the original draft and edited the manuscript for review.

Notes

The authors declare no competing financial interest.

■ ACKNOWLEDGMENTS

This work was funded by the National Science and Technology Major Project of China (2025ZD0551500), the National Natural Science Foundation of China (62501507, 62201446, and 22504112), the Innovation and Technology Fund (ITS/155/24), Xi'an Jiaotong University Medical Development Fund (HX2025137), the Chinese Youth Medical Innovation and Research Project (20251202-01), Xi'an Jiaotong University-College/Enterprise Integrated Innovation Project (YGJC202207), the Young Talent Support Plan of Xi'an Jiaotong University, the Medicine-Engineering Interdisciplinary Research Program (YGJC202207), General Program for Medical Research of Xi'an Science and Technology Plan (2026JH-YXYM-0428) and the China Postdoctoral Science Foundation (2025M781013).

■ REFERENCES

(1) Zhang, J.; Wu, D.; Zeng, F.; Gu, H.; Li, C.; Cata, J. P.; Guo, K.; Miao, C.; Zhang, H. Lactate metabolic reprogramming and histone lactylation modification in sepsis. *Int. J. Biol. Sci.* **2025**, *21*, 5034−5055.

(2) Markwart, R.; Saito, H.; Harder, T.; Tomczyk, S.; Cassini, A.; Fleischmann-Struzek, C.; Reichert, F.; Eckmanns, T.; Allegranzi, B. Epidemiology and burden of sepsis acquired in hospitals and intensive care units: A systematic review and meta-analysis. *Intensive Care Med.* **2020**, *46*, 1536−1551.

(3) Yang, K.; Fan, M.; Wang, X.; Xu, J.; Wang, Y.; Gill, P. S.; Ha, T.; Liu, L.; Hall, J.V.; Williams, D. L.; et al. Lactate induces vascular permeability via disruption of VE-cadherin in endothelial cells during sepsis. *Sci. Adv.* **2022**, *8*, No. eabm8965.

(4) Nuyttens, L.; Vandewalle, J.; Libert, C. Sepsis-induced changes in pyruvate metabolism: Insights and potential therapeutic approaches. *EMBO Mol. Med.* **2024**, *16*, 2678−2698.

(5) Vandewalle, J.; Libert, C. Sepsis: A failing starvation response. *Trends Endocrinol. Metab.* **2022**, *33*, 292−304.

(6) Marbach, J. A.; Di Santo, P.; Kapur, N. K.; Thayer, K. L.; Simard, T.; Jung, R. G.; Parlow, S.; Abdel-Razek, O.; Fernando, S. M.; Labinaz, M.; et al. Lactate clearance as a surrogate for mortality in cardiogenic shock: Insights from the DOREMI trial. *J. Am. Heart Assoc.* **2022**, *11* (6), No. e023322.

(7) Freund, Y.; Cancella de Abreu, M.; Lebal, S.; Rousseau, A.; Lafon, T.; Yordanov, Y.; Macrez, R.; Coisy, F.; Le Borgne, P.; Femy, F.; et al. Effect of the 1-h bundle on mortality in patients with suspected sepsis in the emergency department: A stepped wedge cluster randomized clinical trial. *Intensive Care Med.* **2024**, *50* (10), 1086−1095.

(8) Prescott, H. C.; Antonelli, M.; Alhazzani, W.; Møller, M. H.; Alshamsi, F.; Azevedo, L. C. P.; Belley-Cote, E.; De Waele, J.; Derde, L.; Dionne, J. C.; et al. Surviving Sepsis Campaign: International Guidelines for Management of Sepsis and Septic Shock 2026. *Crit. Care Med.* **2026**, *54* (5), 725−812.

(9) Hu, B.; Chen, J. C. Y.; Dong, Y.; Frank, R. D.; Passe, M.; Portner, E.; Peng, Z. Y.; Kashani, K. Effect of initial infusion rates of fluid resuscitation on outcomes in patients with septic shock: A historical cohort study. *Crit. Care* **2020**, *24* (1), 137.

(10) Ahlstedt, C.; Sivapalan, P.; Kriz, M.; Jacobson, G.; Sylvest Meyhoff, T.; Skov Kaas-Hansen, B.; Holm, M.; Hollenberg, J.; Nalos,

Downloaded from pubs.acs.org/ancac3/article-pdf/20/42/28602/6882571 2/acsnano.6c12805.pdf by CITY UNIV OF HONG KONG user on 11 November 2026

M.; Rooijackers, O.; et al. Effects of restrictive fluid therapy on the time to resolution of hyperlactatemia in ICU patients with septic shock. A secondary post hoc analysis of the CLASSIC randomized trial. *Intensive Care Med.* **2024**, *50* (5), 678−686.
(11) Martin-Loeches, I.; Singer, M.; Leone, M. Sepsis: Key insights, future directions, and immediate goals. A review and expert opinion. *Intensive Care Med.* **2024**, *50*, 2043−2049.
(12) Gambhir, S. S.; Ge, T. J.; Vermesh, O.; Spitler, R.; Gold, G. E. Continuous health monitoring: An opportunity for precision health. *Sci. Transl. Med.* **2021**, *13*, No. eabe5383.
(13) Kim, M. J.; Lasalde-Ramírez, J. A.; Heng, W. Z.; Gao, W. Biomolecular profiling for noninvasive health monitoring. *Nat. Biotechnol.* **2026**, *44*, 934−947.
(14) Chen, L.; Su, B.; Zhong, G.; Wang, J.; Ji, Y.; Zhou, Z.; He, X.; Xu, T. Controlled sweat generation via ultrasound stimulation integrated in a wearable device. *Nat. Commun.* **2026**, *17*, 6954.
(15) Wang, X.; Wang, Y.; Li, Y.; Sun, Y.; Mao, P.; Liu, S.; Ou, J.; Wang, X.; Ren, F.; Zhang, H. Real-time nanomolar vitamin monitoring in sweat using an electrochemical skin-attached device. *Nat. Commun.* **2026**, *17*, 5610.
(16) Min, J.; Tu, J.; Xu, C.; Lukas, H.; Shin, S.; Yang, Y.; Solomon, S. A.; Mukasa, D.; Gao, W. Skin-interfaced wearable sweat sensors for precision medicine. *Chem. Rev.* **2023**, *123*, 5049−5138.
(17) Childs, A.; Mayol, B.; Lasalde-Ramírez, J.A.; Song, Y.; Sempionatto, J. R.; Gao, W. Diving into sweat: Advances, challenges, and future directions in wearable sweat sensing. *ACS Nano.* **2024**, *18*, 24605−24616.
(18) Sempionatto, J. R.; Lin, M.; Yin, L.; de la Paz, E.; Pei, K.; Sonsa-Ard, T.; de Loyola Silva, A. N.; Khorshed, A. A.; Zhang, F.; Tostado, N.; et al. An epidermal patch for the simultaneous monitoring of haemodynamic and metabolic biomarkers. *Nat. Biomed. Eng.* **2021**, *5* (7), 737−748.
(19) Bandodkar, A. J.; Gutruf, P.; Choi, J.; Lee, K.; Sekine, Y.; Reeder, J. T.; Jeang, W. J.; Aranyosi, A. J.; Lee, S. P.; Model, J. B.; et al. Battery-free, skin-interfaced microfluidic/electronic systems for simultaneous electrochemical, colorimetric, and volumetric analysis of sweat. *Sci. Adv.* **2019**, *5*, No. eaav3294.
(20) Yu, Q.; Wu, J.; Xiao, W.; Zhao, C.; Zhang, W.; Chen, Y.; Liu, Y.; Liu, H.; Zhou, J.; Ding, L.; Ju, H. An integrated, wearable paper microfluidic array device for multicomponent electrochemical sweat sensing. *Cell Rep. Phys. Sci.* **2025**, *6*, 102389.
(21) Cho, S.; Shaban, S. M.; Song, R.; Zhang, H.; Yang, D.; Kim, M. J.; Xiong, Y.; Li, X.; Madsen, K.; Wapnick, S.; et al. A skin-interfaced microfluidic platform supports dynamic sweat biochemical analysis during human exercise. *Sci. Transl. Med.* **2024**, *16*, No. eado5366.
(22) Li, M.; Wang, L.; Liu, R.; Li, J.; Zhang, Q.; Shi, G.; Li, Y.; Hou, C.; Wang, H. A highly integrated sensing paper for wearable electrochemical sweat analysis. *Biosens. Bioelectron.* **2021**, *174*, 112828.
(23) Yin, L.; Cao, M.; Kim, K. N.; Lin, M.; Moon, J. M.; Sempionatto, J. R.; Yu, J.; Liu, R.; Wicker, C.; Trifonov, A.; Zhang, F.; Hu, H.; Moreto, J. R.; Go, J.; Xu, S.; Wang, J. A stretchable epidermal sweat sensing platform with an integrated printed battery and electrochromic display. *Nat. Electron.* **2022**, *5*, 694−705.
(24) Xu, Y.; de la Paz, E.; Paul, A.; Mahato, K.; Sempionatto, J. R.; Tostado, N.; Lee, M.; Hota, G.; Lin, M. Y.; Uppal, A.; Chen, W.; Dua, S.; Yin, L.; Wuerstle, B. L.; Deiss, S.; Mercier, P.; Xu, S.; Wang, J. S.; Cauwenberghs, G. In-ear integrated sensor array for the continuous monitoring of brain activity and of lactate in sweat. *Nat. Biomed. Eng.* **2023**, *7*, 1307−1320.
(25) Hasimoto, L. H.; Bridges, M. D.; Perfecto, T. M.; Santhiago, M.; Henry, C. S. Stretchable Laser-induced graphene electrodes for high-performance electrochemical biosensing of lactate in sweat. *ACS Sens.* **2026**, *11*, 2218−2231.
(26) Zhan, Y.; Kim, S.-R.; Song, Y.; Davis, N.; Gillan, L.; Hakola, E.; Mäyrä, A.; Cho, S.; Hiltunen, J.; Javey, A. Wearable optical-electrical skin sensing platform for sweat gland dynamics monitoring. *Nat. Sens.* **2026**, *1*, 494−501.
(27) Zhou, Y.; Nan, F.; Li, Z.; Yin, T.; Cai, B.; Huang, D.; Wang, L.; Yu, W. W. High-performance graphdiyne oxide/Au nanoparticle electrode for electrochemical non-enzymatic glucose sensor. *ACS Nano.* **2025**, *19*, 25262−25272.
(28) Djassemi, O.; Chang, A.-Y.; McGuire, W. C.; Mitchell, E.; Saha, T.; Fernandes, T.; Yang, J.; Miller, M.; Wurster, C.; Morales-Fermin, S.; McGregor, I.; Castillo-Valdovinos, J.; Malhotra, A.; Wang, J. Clinical evaluation of microneedle biosensors for continuous lactate monitoring in critically ill patients. *ACS Sens.* **2026**, *11*, 1413−1424.
(29) Hu, C.; Liang, R.; Li, P.; Ma, Y.; Xie, Y.; Liu, S.; Wang, L.; Peng, M.; Shen, B.; Ren, X.; et al. Bioresorbable electrochemical sensors for continuous deep-tissue lactate monitoring in critical care. *Nat. Commun.* **2026**, *17*, 7366.
(30) Rajendran, J.; Pei, X.; Chakoma, S.; Ghandehari, A.; Tavares-Negrete, J. A.; NajafiKhoshnoo, S.; Esfandyarpour, R.Wireless and in situ regenerable multimodal wearable bioelectronic sweat sensor for continuous biomarker monitoring in everyday settings.*Nat. Biomed. Eng.***2026**
(31) He, W.; Wang, C.; Wang, H.; Jian, M.; Lu, W.; Liang, X.; Zhang, X.; Yang, F.; Zhang, Y. Integrated textile sensor patch for real-time and multiplex sweat analysis. *Sci. Adv.* **2019**, *5*, No. eaax0649.
(32) Tian, H.; Wang, L.; Yang, W.; Li, K.; Zhang, Q.; Li, Y.; Wang, H.; Hou, C. Hierarchical fermat helix-structured electrochemical sensing fibers enable sweat capture and multi-biomarker monitoring. *Mater. Horiz.* **2023**, *10*, 5192−5201.
(33) Niu, J.; Lin, S.; Chen, D.; Wang, Z.; Cao, C.; Gao, A.; Cui, S.; Liu, Y.; Hong, Y.; Zhi, X.; et al. A fully elastic wearable electrochemical sweat detection system of tree-bionic microfluidic structure for real-time monitoring. *Small* **2024**, *20*, 2306769.
(34) Jin, M.; Su, P.; Huang, X.; Zhang, R.; Xu, H.; Wang, Z.; Su, C.; Katona, J. M.; Ye, Y. Micropatterned polymer nanoarrays with distinct superwettability for a highly efficient sweat collection and sensing patch. *Small* **2024**, *20*, 2311380.
(35) Zhou, L.; Li, C.; Luo, Y.; Liang, Q.; Chen, Y.; Yan, Z.; Qiu, L.; He, S. An autonomous fabric electrochemical biosensor for efficient health monitoring. *Natl. Sci. Rev.* **2025**, *12*, No. nwaf155.
(36) Shitanda, I.; Ozone, Y.; Morishita, Y.; Matsui, H.; Loew, N.; Motosuke, M.; Mukaimoto, T.; Kobayashi, M.; Mitsuhara, T.; Sugita, Y.; Matsuo, K.; Yanagita, S.; Suzuki, T.; Mikawa, T.; Watanabe, H.; Itagaki, M. Air-bubble-insensitive microfluidic lactate biosensor for continuous monitoring of lactate in sweat. *ACS Sens.* **2023**, *8*, 2368−2374.
(37) Xu, C.; Song, Y.; Sempionatto, J. R.; Solomon, S. A.; Yu, Y.; Nyein, H. Y. Y.; Tay, R. Y.; Li, J. H.; Heng, W. Z.; Min, J. H.; Lao, A.; Hsiai, T. K.; Sumner, J. A.; Gao, W. A physicochemical-sensing electronic skin for stress response monitoring. *Nat. Electron.* **2024**, *7*, 168−179.
(38) Odinotski, S.; Dhingra, K.; GhavamiNejad, A.; Zheng, H.; GhavamiNejad, P.; Gaouda, H.; Mohammadrezaei, D.; Poudineh, M. A conductive hydrogel-based microneedle platform for real-time pH measurement in live animals. *Small* **2022**, *18*, 2200201.
(39) Li, M.; Li, G.; Xu, T.; Wang, Y.; Xu, R.; Zhang, X.; Chen, F.; Yu, N.; Tian, M. Multi-biosensing hairband for emergency health assessment. *Nat. Commun.* **2025**, *16*, 7224.
(40) Zhang, Y. Y.; Zhang, S. H.; Yang, Y.; Tao, L.; Yu, F. F.; Song, C. Y.; Guo, K.; Zhu, J.; Lin, Y.; Yang, F. R.; et al. A wireless sweat sensing with a pH-based correlation model for continuous glucose monitoring and diabetes management during exercise. *Proc. Natl. Acad. Sci. U. S. A.* **2026**, *123* (11), No. e2532127123.
(41) Tu, J.; Yeom, J.; Ulloa, J. C.; Solomon, S. A.; Min, J.; Heng, W.; Kim, G.; Dao, J.; Vemu, R.; Pang, M.; et al. Stressomic: A wearable microfluidic biosensor for dynamic profiling of multiple stress hormones in sweat. *Sci. Adv.* **2025**, *11*, No. eadx6491.
(42) Tu, J.; Min, J.; Song, Y.; Xu, C.; Li, J.; Moore, J.; Hanson, J.; Hu, E.; Parimon, T.; Wang, T. Y.; Davoodi, E.; Chou, T. F.; Chen, P.; Hsu, J. J.; Rossiter, H. B.; Gao, W. A wireless patch for the monitoring of C-reactive protein in sweat. *Nat. Biomed. Eng.* **2023**, *7*, 1293−1306.
(43) Shin, S.; Gao, W. Making sweat measurable: Induction, sampling, and refreshment in wearable biofluid sensing. *Adv. Sci.* **2026**, No. e75684.

Downloaded from pubs.acs.org/ancac3/article-pdf/20/42/28602/6882571 2/acsnano.6c12805.pdf by CITY UNIV OF HONG KONG user on 11 November 2026

https://doi.org/10.1021/acsnano.6c12805
ACS Nano 2026, 20, 28602−28616

(44) Gattinoni, L.; Vasques, F.; Camporota, L.; Meessen, J.; Romitti, F.; Pasticci, I.; Duscio, E.; Vassalli, F.; Forni, L. G.; Payen, D.; Cressoni, M.; Zanella, A.; Latini, R.; Quintel, M.; Marini, J. J. Understanding lactatemia in human sepsis potential impact for early management. *Am. J. Respir. Crit. Care Med.* **2019**, *200*, 582−589.
(45) Moseley, I.; Correa, A. Lactate and atrial fibrillation risk in ICU patients. *EP Europace* **2026**, *28*, No. euag105.1162.
(46) Duse, D.; Ganea, A.; Horn, P.; Kelm, M.; Jung, C.; Erkens, R. Acidemia is associated with a higher mortality independently of lactate levels in cardiac arrest patients. *Eur. Heart J.* **2025**, *46*, No. ehaf784.2187.
(47) Mi, Y.; Burnham, K. L.; Charles, P. D.; Heilig, R.; Vendrell, I.; Whalley, J.; Torrance, H. D.; Antcliffe, D. B.; May, S. M.; Neville, M. J.; et al. High-throughput mass spectrometry maps the sepsis plasma proteome and differences in patient response. *Sci. Transl. Med.* **2024**, *16* (750), No. eadh0185.
(48) Helleberg, J.; Sundelin, A.; Soltani, N.; Rooyackers, O.; Mårtensson, J. Predictive validity of daily sequential organ failure assessment (SOFA)-2 score for 30-day mortality. *Crit. Care* **2026**, *30*, 280.
(49) Iwasaki, Y.; Kinoshita, T.; Yoshimura, J.; Maruyama, S.; Ohshimo, S.; Murao, S.; Watanabe, M.; Uchida, K.; Igarashi, Y.; Nishimoto, Y.; et al. Admission-day SOFA-2 versus SOFA for mortality discrimination: External validation in a large multicenter ICU database. *Crit. Care* **2026**, *30*, 260.
(50) Wei, S.; Wang, T.; Li, C.; Zhu, Y.; Fan, W.; Ren, H.; Fang, W.; Chen, M. SOFA-2 score predicts mortality in pneumonia-associated sepsis: A retrospective cohort study. *Crit. Care* **2026**, *30*, 302.

Downloaded from pubs.acs.org/ancac3/article-pdf/20/42/28602/6882571 2/acsnano.6c12805.pdf by CITY UNIV OF HONG KONG user on 11 November 2026

https://doi.org/10.1021/acsnano.6c12805
ACS Nano 2026, 20, 28602−28616